Mesons in a Covariant Constituent-Quark Formalism

Sofia C. A. Leitão

Centro de Física Teórica de Partículas. Instituto Superior Técnico - Universidade Técnica de Lisboa
Avenida Rovisco Pais, 1, 1049-001 Lisboa, Portugal
November, 2012

The subject of this work is the study of one of the smallest, yet rather complex systems known in nature: the mesons. We start by treating the mesons as valence quark-antiquark pairs interacting through a static potential and solve the corresponding nonrelativistic Schrödinger equation. We compute mass spectra and wave functions. This first set of calculations confirmed that a nonrelativistic description is adequate for the heavy mesonic sector, while it is not valid for mesons made of light quarks. We perform those calculations in momentum space, where the relativistic kinetic energy and interactions are more naturally formulated, and for general angular momentum states. These calculations serve as preparation for later relativistic calculations. The momentum-space calculations have difficulties originated by singularities in the kernel. We introduced new numerical methods involving sophisticated subtraction methods which enable us to solve the confinement problem in momentum space without using a screening parameter, which is often considered necessary for a numerical solution. We also implemented and tested different numerical methods aiming at high precision.

1 Introduction

Mesons are hadronic particles composed of quarks and gluons, bound together by the strong interaction. Their study is interesting not only for the understanding of the effective nuclear force, between nucleons and nuclei, but also to get more insight into the unique properties of the elementary strong interaction. In fact, an open question of great importance is to understand the connection between the strong interaction acting between elementary quarks, as described by gluon exchange, and the emergence of confinement in hadrons. The answer to this question elucidates on how complex systems can be constructed from elementary ones. It should be emphasized that the confinement interaction has a unique many-body dynamics compared with the dynamics involved in the clustering of nucleons to nuclei or in the clustering of atoms to molecules. This is due to the self-interacting non-linear character of the gluons in non-abelian QCD. It is also worth mentioning that although QCD is widely believed to be the fundamental field theory of the strong interaction, because of the large value of its coupling constant in the low and medium energy regime, it becomes very difficult to solve it, because one cannot use perturbation theory. It is thus necessary to develop other approaches.

Our main and general motivation in this work is to create, in the near future, a unified and consistent relativistic model for mesons as quark-antiquark bound states that can be applied to both heavy and light mesons. The model should satisfy a number of important requirements: (i) the formalism used should be covariant, which is essential for the description of systems composed of light quarks; (ii) the quarks should be strictly confined; (iii) the structure of the constituent quarks themselves, i.e., their self-interaction, should be described consistently through the same confining interaction that acts between pairs of quarks; and (iv) the model should reflect the requirements of chiral symmetry (i.e. when the bare mass of a quark q_i approaches zero, a massless $q_i\bar{q}_i$ bound state must emerge). In the process, knowledge on both the Dirac structure of the effective confinement interaction and the form of the low energy effective one-gluon-exchange interaction is to be gained.

This is of great interest because it will support the analysis of emerging spectroscopic data collected in current and planned experimental activities in Europe and in the USA, for a extensive search for exotic mesons, with a structure that is not reduced to a quark-antiquark pair. Moreover, there are two other possible applications that we can highlight: i) the computation of the pion transition form factor, a necessary input for the hadronic contribution to the anomalous magnetic moment of the muon, which is nowadays being investigated for possible signs of Physics beyond the Standard Model[1]; ii) the production of lepton pairs whose precise knowledge is mandatory in the search for the quark-gluon plasma[2].

The formalism that we will concentrate upon is the so-called Covariant Spectator Theory[3–5] (CST). The work of Gross and Milana[6] (GM) applied the CST for the first time to the study of mesons. CST is based on Relativistic Quantum Field Theory and has been widely and very successfully used in different types of few-body systems, in particular problems involving few nucleons. For a recent review of the CST theory one should see ref.[7]. The model has unique properties since it is entirely covariant and treats confinement and spontaneous breaking of the chiral symmetry in a consistent way. Its final goal is to describe all the mesonic spectrum, from the π to the Υ, providing a robust and useful theoretical basis in which interesting mesonic properties can be computed. However, in the numerical calculations performed so far, the constituent

quark mass has been treated as a constant[6,8,9] or as a phenomenological function not related to the kernel[10]. On of our aims is to correct this deficiency in future work.

In this work we deal with technical numerical difficulties which arise very quickly, even in simpler approaches than the GM model and we treat and test them extensively. Finding new and more efficient solutions to some of these technical difficulties is one of the major contributions of this thesis which, undoubtedly, serves as an important preparatory work to establish, in the near future, a code for reliable predictions of masses of pure $q\bar{q}$ pairs, which is necessary for a definite identification of hybrid states.

2 Formalism

The framework we are interested to work in is based on the CST. The idea behind this theory is that the relativistic series of Feynman diagrams describing any nuclear process can always be reorganized so that only the particles which are interacting are *off-mass-shell*, and all the other particles, which are *spectators* to the interaction, are considered *on-mass-shell*.

In the literature a first work that developed this idea is found in ref.[3], where integral equations particularly suitable to the dynamical treatment of strongly interacting particles are derived. These equations were deduced from the Bethe-Salpeter equation following one major assumption:

All the particles of a system, but one, are on the-mass-shell for all the intermediate states. The on-mass-shell particles are viewed, and called, as "spectators" of an interaction vertex. It is the off-mass-shell particle that participates in the vertex of the interaction.

As a consequence of this assumption the complete kernel of the four-dimensional Bethe-Salpeter equation is turned into an equivalent form, with a different propagator and a kernel modified accordingly. The new propagator is chosen such that, when the kernel of the reorganized equation is truncated to include ladder terms only, the dimension of the integration over intermediate momenta reduces from four to three, while maintaining the covariance of the equation.

This underlying principle of the CST is originally motivated by a very interesting observation: a partial but important *cancellation* occurs between the two-body box and crossed-box diagrams in scalar theories of ϕ^3-type. This cancellation implies that the only terms that survive in any iteration of the exact ladder and crossed ladder terms are the ladder diagrams with one particle on-mass-shell in all intermediate states. At the end, therefore, the integral equation that is obtained sums only ladder diagrams with one particle on-mass-shell in any intermediate state, and consequently is a 3-dimensional reduction of the 4-dimensional Bethe-Salpeter equation. This way, we overcome the impossibility of summing an infinite series of diagrams and get a better approximation by summing only ladder terms where one particle is on mass-shell in all internal loops.

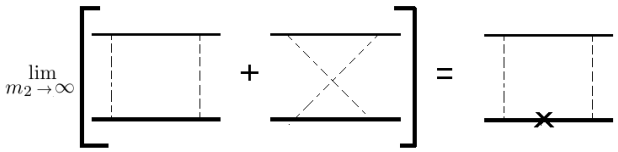

Fig. 1 Illustration of the cancellation theorem. The cross means that the heaviest particle is on its mass shell.

2.1 A CST model for mesons

The GM model[6] is the first covariant model that appeared as an application of the CST to the bound state of a quark+antiquark system. We review here the main features of this model:

1. Mesons are interpreted as bound-states of a quark and an antiquark, either one of which can be *off-shell*. The model is a **relativistic** generalization of the nonrelativistic (or semirelativistic) models of Godfrey and Isgur[11].

2. The relativistic bound state equation is written in momentum space, where nonlocalities and energy dependences of the interactions can be taken into account more easily.

3. The **confining potential** has a **linear part** that is known to emerge, in the quenched approximation, from lattice QCD calculations, and a **constant part** that enables an adjustment of the overall energy scale. In momentum space this potential has a leading term in q^{-4}, that is regularized by subtracting the leading singularity at $q^2 = 0$. This potential is multiplied by a $\lambda_1.\lambda_2$ factor to account for the color part. In this sense, only the color singlets are confined.

4. The spin-dependent structure of the confining potential is chosen to be consistent with **chiral symmetry**. The authors explored the *simplest* case of chiral symmetry under the $SU(2) \times SU(2)$ group and also under the $U(1) \times U(1)$ group case.

5. Following the ideas of NJL models[12] in which chiral symmetry is spontaneously broken, the constituent quark mass arises dynamically from its self-interaction with the confining forces. Considering the pion, its nonzero mass is theoretically a natural consequence of **chiral symmetry breaking** generating a sizable quark mass from the originally almost zero bare quark mass of the QCD Lagrangian. However, in the numerical calculations, this consistency between confinement and chiral symmetry was not yet fully implemented.

6. In the relativistic equation for the bound state the relative energy variable is constrained by restricting one

of the quark to its positive energy mass-shell — this is called the one-channel case. This means that despite the fact that the equations are covariant, they depend, like nonrelativistic equations, on the relative three momentum only and have a smooth nonrelativistic limit so they are expected to describe most accurately the **heavy-light** deeply bound systems.

7. For the case of **not very deeply bound states**, two channels have to be included, one with the quark on its positive-energy mass-shell and one with the antiquark on its negative energy mass-shell. This point will be seen in more detail on the next section.

2.2 The one-channel vertex spectator 1CS equation

Following the features just described, we take here the meson as a bound state of a quark and an anti-quark, and write down the Feynman diagram for the bound state meson vertex equation has shown in Fig.(2).

Particle 1 is the quark, particle 2 the antiquark and $\mathscr{O}$ is a matrix in the Dirac space that describes how the confining force couples to the quark or antiquark. The kernel V contains the momentum dependent structure of the confining potential. The equations are derived in the center of mass rest frame, where $P=(\mu,\mathbf{0})$.

Later, the quark (particle 1) will be placed on shell, thus producing the single channel equation. The four momenta used in the diagram in terms of the total four-momentum $P=p_1-p_2$, and the relative momentum $p=\frac{1}{2}(p_1+p_2)$ are:

$$\begin{aligned} &\text{final state:} && p_1=p+\frac{1}{2}P \quad p_2=p-\frac{1}{2}P, \\ &\text{internal loop:} && k_1=k+\frac{1}{2}P \quad k_2=k-\frac{1}{2}P, \end{aligned} \tag{1}$$

where p_1 refers to the quark and p_2 refers to the anti-quark (which has a minus sign).

The vector k is the relative internal momentum of the quark-antiquark pair, in an intermediate state.

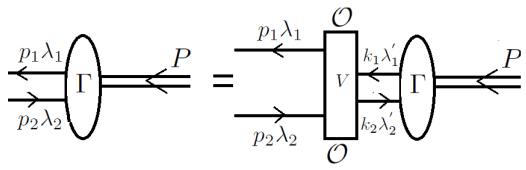

Fig. 2 Diagrammatic representation of the Bethe-Salpeter equation for the meson bound-state vertex function Γ. The kernel, or potential, is denoted by V.

The two fermion propagators have poles that can be represented in the complex plane k_0. Factoring the denominators of the propagators as:

$$\frac{1}{m_i^2-k_i^2}=G_i^+G_i^-, \tag{2}$$

we have the following poles (labeled as suggested below) and the corresponding singularities.

$$\begin{aligned} &1: \quad \left(G_1^+\right)^{-1}=E_{k1}-\left(k_0+\frac{1}{2}\mu\right)-i\varepsilon: && k_0=E_{k1}-\frac{1}{2}\mu-i\varepsilon \\ &2: \quad \left(G_2^+\right)^{-1}=E_{k2}-\left(k_0-\frac{1}{2}\mu\right)-i\varepsilon: && k_0=E_{k2}+\frac{1}{2}\mu-i\varepsilon \\ &3: \quad \left(G_1^-\right)^{-1}=E_{k1}+\left(k_0+\frac{1}{2}\mu\right)-i\varepsilon: && k_0=-E_{k1}-\frac{1}{2}\mu+i\varepsilon \\ &4: \quad \left(G_2^-\right)^{-1}=E_{k2}+\left(k_0-\frac{1}{2}\mu\right)-i\varepsilon: && k_0=-E_{k2}+\frac{1}{2}\mu+i\varepsilon. \end{aligned} \tag{3}$$

They are represented in Fig.(3).

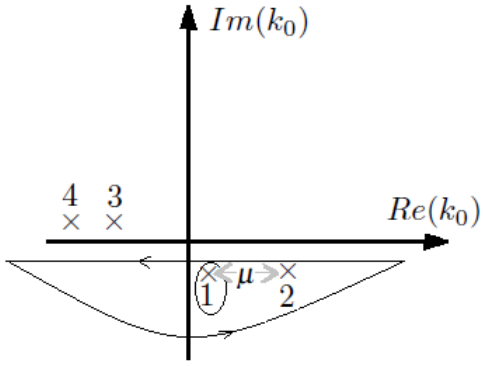

Fig. 3 Position of the four poles associated with the four propagators G_i^ρ in the bound state equation.

Performing the k_0 integration in a closed contour in the lower half plane, we may keep only the residue from the dominant pole, pole 1. This is a good approximation when μ large, since then pole 1 is in the close vicinity of pole 3 — where the integrand is large — and therefore 1 is the dominating contribution from the lower half plane poles. When μ is small pole 2 should also be included, just as discussed on point 7 of the previous section. With these considerations one obtains:

$$\Gamma(p)=-\int\frac{d^3k}{2E_{k1}(2\pi)^3}V(p,k)\mathscr{O}(m_1+\not{\hat{k}}_1)\Gamma(k)\frac{m_2+\not{k}_2}{m_2^2-k_2^2}\mathscr{O}, \tag{4}$$

where now* $\hat{k}_1=(E_{k1},\mathbf{k})$ and $k_2=(E_{k1}-\mu,\mathbf{k})$.

This is one form of the **One Channel Spectator equation**, labeled for short, the **1CS** equation.

* The hat on k_1 means the particle is on-shell.

Recalling that the projection operator[13] can be written[†] as a sum over on-shell u spinors, we have:

$$m_1 + \not{k}_1 = \sum_{\lambda'} u\left(\mathbf{k},\lambda'\right)\bar{u}\left(\mathbf{k},\lambda'\right), \tag{5}$$

where λ is the eigenvalue of the Helicity operator in the Helicity representation. Defining now the relativistic meson wave function as

$$\Psi(k,\lambda) = \frac{1}{\sqrt{2E_{k1}}}\bar{u}(\mathbf{k},\lambda)\Gamma(k)\frac{m_2 + \not{k}_2}{m_2^2 - k_2^2}, \tag{6}$$

Eq. (4) becomes:

$$\Psi(p,\lambda)(m_2 - \not{p}_2) = -\int \frac{d^3k}{(2\pi)^3}\frac{V(p,k)}{\sqrt{4E_{p1}E_{k1}}} \times \sum_{\lambda'} \bar{u}(\mathbf{p},\lambda)\mathscr{O}u\left(\mathbf{p},\lambda'\right)\Psi(k,\lambda')\mathscr{O}. \tag{7}$$

In this work, we have investigated Eq.(7) further. In particular, we have shown that the one-body limit of this equation is the Dirac equation, for the light quark moving in the presence of the infinitely heavy one, when one takes the ratio between the two constituent masses tend to infinity. We have seen and we will show in Section 5 that the results from the 1CS equation coincide with the non-relativistic Schrödinger results when both masses are very large. The success in obtaining this limit shows that both the 1CS equation and the relativistic kernel for the confining interaction have the correct nonrelativistic limit.

Finally, the main applications of the model will be listed and procedures to improve upon the 1CS equation will be presented. It is important to keep in mind though, that some of these aspects are currently under development.

3 Nonrelativistic Schrödinger Equation (NRSE) in momentum space

Before attempting to solve Eq.(7) we studied a simpler yet instructive problem: the NRSE in momentum space with a linear confining potential (which will then be properly generalized to the relativistic case for the 1CS equation):

$$\frac{p^2}{2m_R}\langle\mathbf{p}|\psi\rangle + \int \frac{d^3k}{(2\pi)^3}\langle\mathbf{p}|V_L|\mathbf{k}\rangle\langle\mathbf{k}|\psi\rangle = E\langle\mathbf{p}|\psi\rangle, \tag{8}$$

where m_R is the reduced mass of the *quark-anti-quark* system and $\mathbf{p}$ and $\mathbf{k}$ are the incoming and outgoing relative momenta. The linear potential[6] is given by

$$V_L(\mathbf{q}) = V_A(\mathbf{q}) - (2\pi)^3\delta^{(3)}(\mathbf{q})\int \frac{d^3\mathbf{q}'}{(2\pi)^3}V_A(\mathbf{q}'), \tag{9}$$

where $\mathbf{q}$ is the momentum transfer, and

$$V_A(\mathbf{q}) = -\frac{8\pi\sigma}{\mathbf{q}^4}. \tag{10}$$

After performing a partial-wave decomposition we arrived at the following equation for a general angular momentum l:

$$\frac{p^2}{2m_R}\psi_l(p) - \frac{2\sigma}{\pi}\int_0^\infty dk\left\{\frac{2k^2}{(k^2-p^2)^2}\left[P_l(y)\psi_l(k) - \psi_l(p)\right] + \frac{w'_{l-1}(y)}{2p^2}\psi_l(k) - \frac{1}{4p^2}\ln\left(\frac{p+k}{p-k}\right)^2 P'_l(y)\psi_l(k)\right\} = E\psi_l(p) \tag{11}$$

where $P_l(y)$ is the l^{th} Polynomial of Legendre of first kind,$w_{l-1}(y)$ is given by

$$w_{l-1}(y) = \sum_{m=1}^{l}\frac{1}{m}P_{l-m}(y)P_{m-1}(y), \tag{12}$$

and

$$y = \frac{p^2+k^2}{2pk}. \tag{13}$$

Analyzing the kernel of Eq.(11) we see that it is singular at $k = p$. Regarding the first term of the integrand, it appears to have a double pole, but, because the factor in brackets that multiplies the numerator goes to zero like $(k-p)$, it is actually a single pole and the principal value integral exists.

Although there are standard numerical methods to solve integral equations with principal-value type singularities, they require special care and typically also more computing time. From the practical point of view it would be a considerable advantage to eliminate those singularities altogether. We manage to achieved this by means of subtraction methods. Furthermore, we explore two different methods to numerically solve these equations: the *SSI* (Splines single integration) and *SDI* (Splines double integration) methods.

4 Implementation of the Numerical Methods

4.1 Removing the singularities

In this section we will outline the main steps required to remove the singularities. In the following it is important to distinguish between the ordinary integral and the Cauchy principal value integral, denoted here by the symbol "$\not\int$".

[†] where $u(\mathbf{p}\lambda) = \sqrt{E_p + m}\begin{pmatrix} 1 \\ \frac{\sigma\cdot\mathbf{p}}{E_p+m}\end{pmatrix}\chi^\lambda$

Thus, considering the most singular part of Eq.(11), which appears in

$$I_1 = \int_0^\infty dk \frac{2k^2}{(k^2-p^2)^2}\left[P_l(y)\psi_l(k) - \psi_l(p)\right]. \quad (14)$$

If one makes a Taylor expansion of the term in brackets around $p = k$, the result in proportional to $(k-p)$ and this cancels one of the powers of the singularity in the denominator. The remaining singularity is a single pole that can be calculated as a Cauchy principal value singularity.

With a second subtraction using the well-known result

$$\int_0^\infty \frac{dp}{k^2-p^2} = 0 \quad (15)$$

we can transform this equation further to a singularity-free equation:

$$I_1 = \int_0^\infty \frac{dk}{k^2-p^2}\left\{\frac{2k^2}{k^2-p^2}\right. \\ \left.[P_l(y)\psi_l(k) - \psi_l(p)] - p\psi_l'(p)\right\}. \quad (16)$$

Note that the modified integrand is now regular at $k = p$ and it is no longer a principal-value but an ordinary integral. The price to pay for this simplification is that the derivative of the wave function enters the integrand. However, this is no significant complication if the method of solving the integral equation uses an expansion of $\psi_l(p)$ into a set of basis functions whose derivatives can be easily calculated.

Next we address the second singular integrand

$$I_2 = -\frac{1}{4p^2}\int_0^\infty dk \ln\left(\frac{p+k}{p-k}\right)^2 P_l'(y)\psi_l(k) = \\ -\frac{1}{2p^2}\int_0^\infty dk\, Q_0(y)P_l'(y)\psi_l(k), \quad (17)$$

where $Q_0(y)$ is the Legendre function of the second kind given for general l by

$$Q_l(y) = \frac{1}{2}\int_{-1}^{1} dx \frac{P_l(x)}{y-x}. \quad (18)$$

Using

$$\int_0^\infty dk \frac{Q_0(y)}{k} = \frac{\pi^2}{2} \quad (19)$$

we can bring I_2 into the following form:

$$I_2 = -\frac{1}{2p^2}\int_0^\infty dk\, Q_0(y)\left[P_l'(y)\psi_l(k)\right. \\ \left. -\frac{p}{k}\frac{l(l+1)}{2}\psi_l(p)\right] - \frac{\pi^2 l(l+1)}{8p}\psi_l(p). \quad (20)$$

The factor in brackets in the integrand is proportional to $(k-p)$ near $k = p$, such that the product $(k-p)Q_0(y)$ goes to zero at that point. The subtracted integrand is therefore also non-singular.

After this procedure, we used the B-splines[14] defined on the interval $[0,1]$ in x and performed the following mapping to move for the p-space:

$$x = \frac{2}{\pi}\arctan\left(\frac{p}{\Lambda}\right), \qquad \Lambda = 1GeV. \quad (21)$$

In order to illustrate the two previously described methods we took here the NRSE for $l = 0$ after our procedure to transform it in a singularity-free equation, i.e,

$$\frac{p^2}{2m_R}\psi(p) - \frac{4\sigma}{\pi}\int_0^\infty dk \frac{k^2}{(k+p)^2(k-p)^2}\cdot \\ \cdot\left[\psi(k) - \psi(p) - \frac{p^2}{2pk^2}(k+p)(k-p)\psi'(p)\right] = E\psi(p), \quad (22)$$

4.2 SSI Method

The **SSI Method** (Splines single integration) uses a set cubic splines $\beta_j(p)$ defined in order to have the appropriate boundary conditions for the different l states. It is called splines single integration method because it only requires single integrations.

Taking the expansion $\psi(p) = \sum_{j=1}^{SN}\alpha_j\beta_j(p)$, the first step involves choosing a proper mesh of points $p_i = 1,...,SN$ so that Eq.(22) can be transformed into:

$$\sum_{j=1}^{SN}\frac{p_i^2}{2m_R}\beta_j(p_i)\alpha_j - \frac{4\sigma}{\pi}\sum_{j=1}^{SN}\int_0^\infty dp \frac{k^2}{(k+p_i)^2(k-p_i)^2}\cdot \\ \cdot\left[\beta_j(k) - \beta_j(p_i) - \frac{p^2(k+p_i)(k-p_i)}{2p_ik^2}\beta_j'(p_i)\right]\alpha_j = E\sum_{j=1}^{SN}\beta_j(p_i)\alpha_j. \quad (23)$$

The mesh was chosen so that the point were equally distributed in $x \in [0,1]$ and then mapped into $p \in [0,\infty[$, However, there's no unique choice and the results obtained are not completely independent from this.

Defining now

$$A_{ij} = \frac{p_i^2}{2m_R}\beta_j(p_i), \quad (24)$$

$$V_{ij} = -\frac{4\sigma}{\pi}\sum_{j=1}^{SN}\int_0^\infty \frac{k^2}{(k+p_i)^2(k-p_i)^2} \\ \times\left[\beta_j(k) - \beta_j(p_i) - \frac{p^2(k+p_i)(k-p_i)}{2p_ik^2}\beta_j'(p_i)\right], \quad (25)$$

and

$$C_{ij} = \beta_j(p_i), \tag{26}$$

we get a generalized eigenvalue problem

$$(A_{ij} + V_{ij})\,\alpha_j = EC_{ij}\alpha_j, \tag{27}$$

where E are the eigenvalues and α_j the corresponding eigenvectors. Finding the set of Es and the corresponding α_j completely defines the problem of finding the binding energies and the wavefunctions for the bound states.

4.3 SDI Method (Splines double integration)

The **SDI method** (Splines double integration) also uses the cubic splines previously defined but now double integrations emerge from the fact that Eq.(22) is multiplied in both sides by the operator

$$\int p^2 \beta_l(p) dp. \tag{28}$$

This is motivated from the Quantum Mechanics' procedure to find the eigenvalues, using the orthogonality of the basis set of functions. In our case, the basis is not orthogonal so the diagonalizing procedure will not be complete. However, we reduce many of the resulting matrix entrances to zero, facilitating the numerical computation of the eigenvalues.

In this case, the generalized eigenvalue problem is

$$\int_0^\infty dp \frac{p^4}{2m_R}\beta_j(p)\beta_l(p)\alpha_j - \\ -\frac{4\sigma}{\pi}\int_0^\infty\int_0^\infty dpdk \frac{p^2k^2}{(k+p)^2(k-p)^2} \\ \left[\beta_j(k)\beta_l(p) - \beta_j(p)\beta_l(p) - \frac{p^2(k+p)(k-p)}{2pk^2}\beta_j'(p)\beta_l(p)\right]\alpha_j = \\ = E\int_0^\infty dp p^2 \beta_j(p)\beta_l(p)\alpha_j. \tag{29}$$

Defining now

$$A_{jl} = \int_0^\infty dp \frac{p^4}{2m_R}\beta_j(p)\beta_l(p)\alpha_j, \tag{30}$$

$$V_{jl} = -\frac{4\sigma}{\pi}\int_0^\infty\int_0^\infty dpdk \frac{p^2k^2}{(k+p)^2(k-p)^2} \\ \times\left[\beta_j(k)\beta_l(p) - \beta_j(p)\beta_l(p) - \frac{p^2(k+p)(k-p)}{2pk^2}\beta_j'(p)\beta_l(p)\right] \tag{31}$$

and

$$C_{jl} = \int_0^\infty dp p^2 \beta_j(p)\beta_l(p) \tag{32}$$

so

$$\left(A_{jl} + V_{jl}\right)\alpha_j = EC_{jl}\alpha_j \tag{33}$$

where once more the E are the eigenvalues and α_j the corresponding eigenvectors and the problem of finding the binding energies and wavefunctions is finished.

5 Results

5.1 NRSE in momentum space

In this section we present the results obtained for the solutions of the NRSE in momentum space.

We start with table 1 by analyzing the consistency between the results obtained in momentum space for the SSI and the SDI methods described in the text and our previous results of the r-space[‡], for the first five excited states of the $l = 0$ case. Globally, we can state the results are consistent, even though the r- space and SDI method are closer to each other than the SSI method for the same number of splines.

In table 2 we make the same analysis for the p and d case. In this situation the method SSI did not provide stable results. But, considering the SDI method, we see that once more the results match in the two spaces.

Since the results for the $l = 0$ case are known and can be determined in terms of the *Airy* function, we investigated the accuracy of our two methods in table 3. The results clearly indicate the SDI method as the most accurate.

Another important issue to address when studying numerical methods of this type is to analyze the rate of convergence. For that one can see in Fig.4 and 5 the relative difference in percentage between the result computed with $SN = 48$ and $SN = 64$ splines as a function of the number of the state. We see that for the SSI Method from around $n = 7$ the values start diverging. On the other hand, for the SDI method, the convergence lasts until approximately $n = 13$. Another interesting feature is that almost cyclically some dips appear, indicating that convergence for some eigenvalues is more easy than others. However, they do not coincide so probably this is related with the intrinsic structure of the method.

Obviously, the general behavior is that the convergence worsens with increasing n and this has a physical reason behind it. This happens because the functions evaluated are successively more oscillant, making the integrations harder. As an illustrative example we plot in Fig.6 and 7 the solutions of wavefunctions corresponding to the ψ_{11}, ψ_{12} and ψ_{13} computed with $SN = 16$ and $SN = 128$. What one notes is that with $SN = 16$ we do not have enough flexibility to represent the right solutions (wavefunctions with 11, 12 and 13 nodes as expected), so a higher number of splines is required. In this case one needs $SN = 128$ to have the desired result.

‡ We have also solved the NRSE equation in configuration space and obtained the mass spectra, which we compared with the experimental meson known masses. However, and for the sake of brevity, we did not present those results here.

E_n	r-space	SSI	SDI
E_1	2.338107	2.338108	2.338108
E_2	4.087949	4.087930	4.087949
E_3	5.520560	5.520397	5.520560
E_4	6.786793	6.786107	6.786708
E_5	7.947376	7.942539	7.944133

Table 1 First binding energies for the s-states. Comparison between the results obtained in the r-space and p-space, for both SSI and SDI method with $SN = 64$.

E_n	r-space	SDI ($l = 1$)	r-space	SDI ($l = 2$)
E_1	3.361254	3.361258	4.248182	4.248181
E_2	4.884452	4.884456	5.629709	5.629706
E_3	6.207632	6.207627	6.868961	6.688798
E_4	7.406265	7.405669	8.012763	8.009610
E_5	8.528377	8.515238	9.117374	9.076910

Table 2 First binding energies for the p-states and d-states. Comparison between the results obtained in the r-space and p-space with the SDI method with $SN = 64$ for the p case and d case.

As a final overall comment, we can say that the SDI Method, has proven to be a robust and efficient method to solve this type of integral equation and if we want to increase the precision or describe higher excited states, we simply have to increase the number of splines in the basis.

E_n	SSI	SDI	-Airy zeros
E_1	2.33810847	2.33810761	2.33810741
E_2	4.08793008	4.08794940	4.08794944
E_3	5.52039730	5.52055962	5.52055983
E_4	6.78610688	6.78670794	6.78670809
E_5	7.94253855	7.94413344	7.94413359
E_6	9.01914089	9.02265121	9.02265085
E_7	10.0333347	10.0401766	10.04017434
E_8	10.9962901	11.0085333	11.00852430
E_9	11.9154774	11.9360443	11.93601556
E_{10}	12.7959345	12.8288595	12.82877675
E_{11}	13.6409344	13.6917101	13.69148904
E_{12}	14.4523266	14.5283875	14.52782995
E_{13}	15.2306641	15.3420908	15.34075514
E_{14}	15.9751412	16.1357142	16.13268516
E_{15}	16.6841443	16.9121212	16.90563400
E_{16}	17.3551871	17.6750887	17.66130011
E_{17}	17.9627796	18.4288721	18.40113260
E_{18}	18.5544209	19.1673236	19.16732359
E_{19}	19.2397772	19.9034692	19.83812989
E_{20}	19.4522432	20.7065084	20.53733291

Table 3 Accuracy of the SSI and SDI methods. The Airy zeros were found with the software Mathematica 7.0. The results were obtained SSI and SDI methods with $SN = 64$.

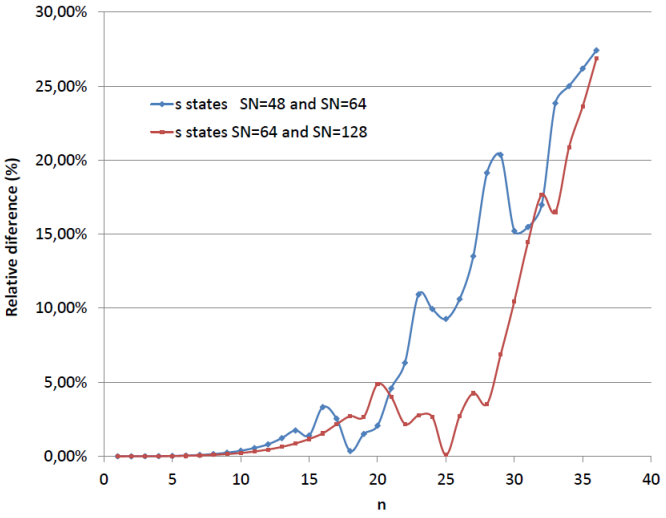

Fig. 4 Study of convergence in SSI Method. This plot represents in the x axis the n principal quantum number of the state and in the y axis the relative differences in % between the binding energies computed with $SN = 48$ and $SN = 64$ (blue) and $SN = 64$ and $SN = 128$ (red).

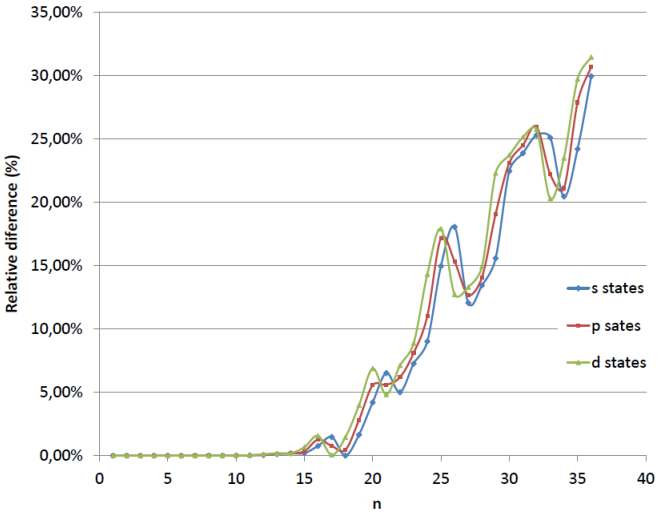

Fig. 5 Study of convergence in SDI Method. This plot represents in the x axis the n principal quantum number of the state and in the y axis the relative differences in % between the binding energies computed with $SN = 48$ and $SN = 64$.

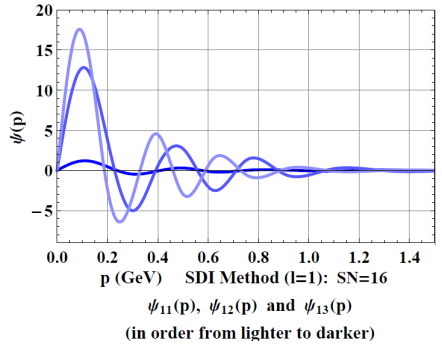

Fig. 6 Normalized wavefunction of ψ_{11}, ψ_{12} and ψ_{13} with $SN = 16$.

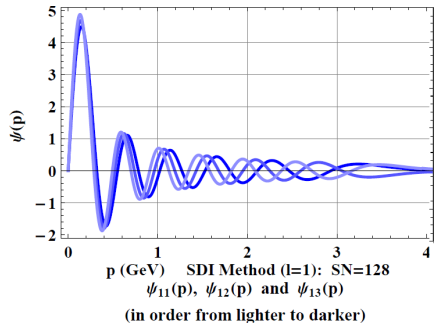

Fig. 7 Normalized wavefunction of ψ_{11}, ψ_{12} and ψ_{13} with $SN = 128$.

Level	In this work	ref.([14])	In this work	ref.([14])
n	$SN = 12$	$SN = 12$	$SN = 20$	$SN = 20$
4	2.11225	2.113	2.10694	2.109
3	1.80699	1.808	1.80727	1.808
2	1.44224	1.443	1.44232	1.443
1	0.93876	0.939	0.93867	0.940
-1	-0.93630	-0.936	-0.93630	-0.936
-2	-1.08500	-1.084	-1.08406	-1.084
-3	-1.17043	-1.170	-1.17296	-1.173
-4	-1.25905	-1.259	-1.23379	-1.233

Table 4 Comparison with ref.([14]) results (in GeV) for the 1CS equation with $\sigma = 0.2 GeV^2$, $\kappa = 5.0$ and m_2=0.325GeV/c^2.

5.2 Dirac and 1CS equation

In this work we chose to solve both the Dirac and the 1CS equation with a scalar linear potential. Our computations were performed in helicity representation for the s-wave case. This choice was made in order to reproduce the results of ref.([14]).

Specifically, in Eq.(7) we have adopted

$$\mathscr{O} \equiv \mathbf{1} \tag{34}$$

and

$$V(p,k) = -8\pi\sigma \left\{ \frac{1}{(p-k)^4} - E_{p_1}\delta^3(p-k) \int \frac{d^3k'}{E_{k_1'}(p-k')^4} \right\}, \tag{35}$$

where the insertion of the energy factors is necessary to make the kernel covariant with the restriction of the heavy quark placed on its mass shell. The full 1CS also includes the covariant replacement $(p-k)^2 \to (E_{p_1} - E_{k_1})^2 - (\mathbf{p}-\mathbf{k})^2$, but in the numerical studies in this work we have neglected retardation and use the simplest replacement $(p-k)^2 \to -(\mathbf{p}-\mathbf{k})^2$ as the authors did in ref.([14]). This is usually called the *quasirelativistic* approximation. In tables 6, 4 and 5 we compare our results for the energy states obtained with those from ref.([14]).

An important parameter is $\kappa = m_1/m_2$, the mass ratio between the heavy quark m_1 and the light quark m_2.

For the CST case we show the results for two cases of the quark mass ratio ($\kappa = 1$ and $\kappa = 10$). The first conclusion is that our results are in very good agreement with the ones published in the literature, and therefore our numerical method passed this first test. Positive and negative energy eigenvalues for the two-quark bound state were found, since the two-body equations are relativistic.

Besides the eigenvalues, we also calculated the eigenvectors of the Dirac and the 1CS equations.

From now on, we will assume the following short-hand no-

Level	In this work	ref.([14])	In this work	ref.([14])
κ	$\kappa = 10.0$	$\kappa = 10.0$	$\kappa = 1.0$	$\kappa = 1.0$
n	$SN = 12$	$SN = 12$	$SN = 12$	$SN = 12$
4	2.07724	2.078	1.88090	1.881
3	1.78248	1.783	1.63183	1.632
2	1.43478	1.435	1.29244	1.293
1	0.96313	0.964	0.74397	0.745
-1	-1.09110	-1.009	-0.33407	-0.334
-2	-1.33336	-1.332	-0.34137	-0.341
-3	-1.51631	-1.515	-0.35430	-0.354
-4	-1.64306	-1.642	-0.37916	-0.379

Table 5 Comparison with ref.([14]) results (in GeV) for 1CS equation with $\sigma = 0.2 GeV^2$ and m_2=0.325GeV/c^2 for $\kappa = 10.0$ and $\kappa = 1.0$.

Level	In this work	ref.([14])
4	1.94618	1.946
3	1.69508	1.695
2	1.39289	1.393
1	0.97542	0.976
-1	-1.24977	-1.248
-2	-1.57576	-1.574
-3	-1.83980	-1.838
-4	-2.08025	-2.078

Table 6 Comparison with ref.([14]) results (in GeV) for the Dirac equation with $\sigma = 0.2 GeV^2$, m_2=0.325GeV/c^2 and $SN = 12$.

tation for the eigenvectors

$$\left(\begin{array}{l} \left(\begin{array}{c} \alpha_1^1 \\ \alpha_2^1 \\ \ldots \\ \alpha_{SN}^1 \end{array} \right) \equiv \overrightarrow{\alpha}^+ \\ \left(\begin{array}{c} \alpha_1^2 \\ \alpha_2^2 \\ \ldots \\ \alpha_{SN}^2 \end{array} \right) \equiv \overrightarrow{\alpha}^- \end{array} \right), \tag{36}$$

$$\phi^+(p) = \sum_{j=1}^{SN} \alpha_j^+ \beta_j(p), \tag{37}$$

$$\phi^-(p) = \sum_{j=1}^{SN} \alpha_j^- \beta_j(p). \tag{38}$$

Since we are dealing with relativistic equations some of the eigenvalues are negative and the upper and lower wavefunction components denoted by ϕ^+ and ϕ^- exist for both positive and negative eigenvalues. In the non-relativistic limit ϕ^- becomes zero as it should - we checked this numerically - since they correspond to the projection of the two-body vertex function into the v-spinor part of the off-shell-quark propagator. We show a series of the Dirac wavefunctions in Figs. 8, 9, 10 and 11; and for the 1CS equation in Figs. 12, 13, 14, 15, 16 and 17. We remark that the number of nodes increases with the energy of the state, as it should. For positive-energy states ϕ^+ dominates over ϕ^-, while for negative-energy states ϕ^- dominates over ϕ^+.

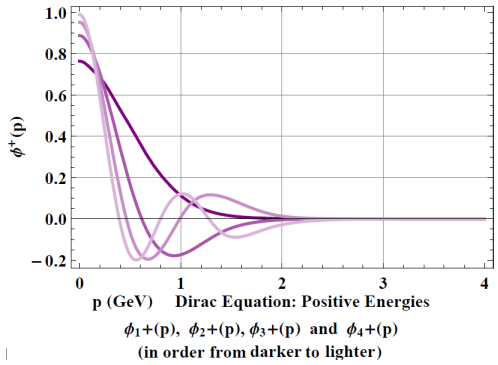

Fig. 8 Dirac $\phi^+(p)$ wavefunctions for the first positive energies. The parameters used were: $\sigma = 0.2 GeV^2$ and $m = 0.325 GeV/c^2$.

5.2.1 1CS One-body (Dirac) Limit In table 7 we show the results of the 1CS equation for the excited states as one increases the mass ratio κ. The values, just as expected, tend to the one-body limit Dirac results, for both positive and negative energies. This is illustrated in Figs.18 and 19.

5.2.2 Non-relativistic reduction of the 1CS and Dirac equations

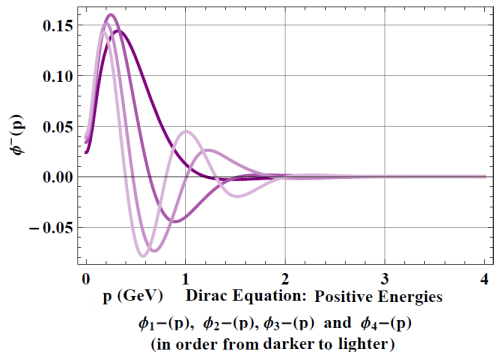

Fig. 9 Dirac $\phi^-(p)$ wavefunctions for the first positive energies. The parameters used were: $\sigma = 0.2GeV^2$ and $m = 0.325GeV/c^2$.

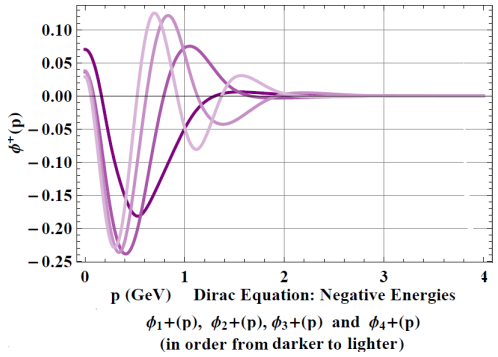

Fig. 10 Dirac $\phi^+(p)$ wavefunctions for the first negative energies. The parameters used were: $\sigma = 0.2GeV^2$ and $m = 0.325GeV/c^2$.

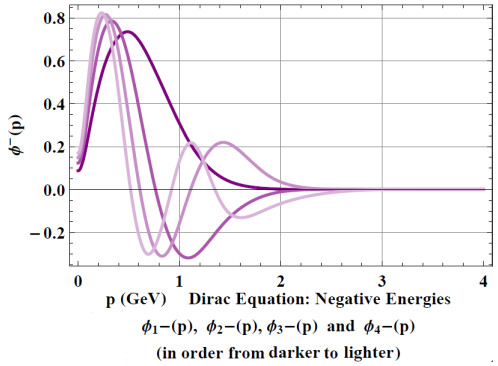

Fig. 11 Dirac $\phi^-(p)$ wavefunctions for the first negative energies. The parameters used were: $\sigma = 0.2GeV^2$ and $m = 0.325GeV/c^2$.

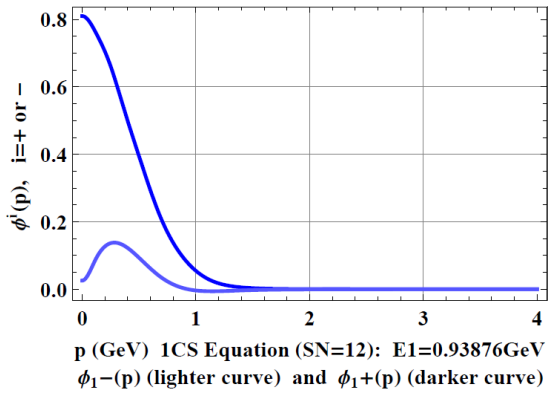

Fig. 12 1CS $\phi^+(p)$ and $\phi^-(p)$ wavefunctions for E_1. The parameters used were: $\sigma = 0.2GeV^2$ and $m = 0.325GeV/c^2$.

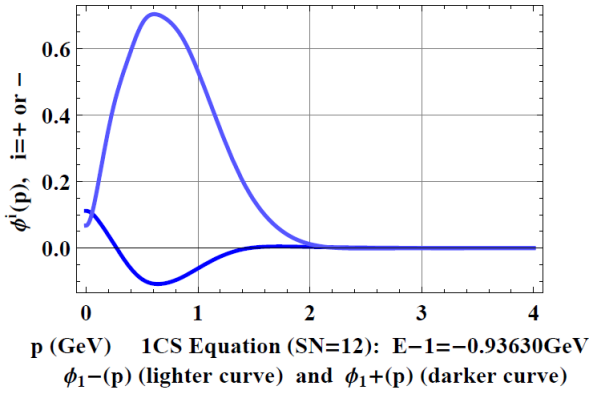

Fig. 13 1CS $\phi^+(p)$ and $\phi^-(p)$ wavefunctions for E_{-1}. The parameters used were: $\sigma = 0.2GeV^2$ and $m = 0.325GeV/c^2$.

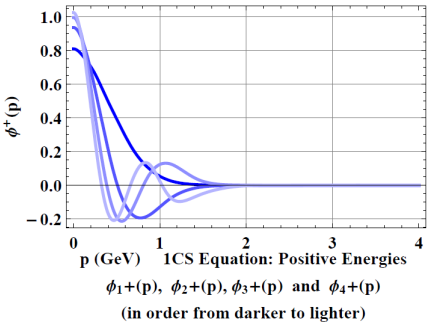

Fig. 14 1CS $\phi^+(p)$ wavefunctions for the first positive energies. The parameters used were: $\sigma = 0.2GeV^2$, $\kappa = 5.0$ and $m_2 = 0.325GeV/c^2$.

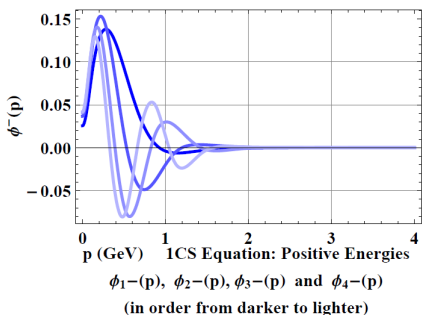

Fig. 15 1CS $\phi^-(p)$ wavefunctions for the first positive energies. The parameters used were: $\sigma = 0.2GeV^2$, $\kappa = 5.0$ and $m_2 = 0.325GeV/c^2$.

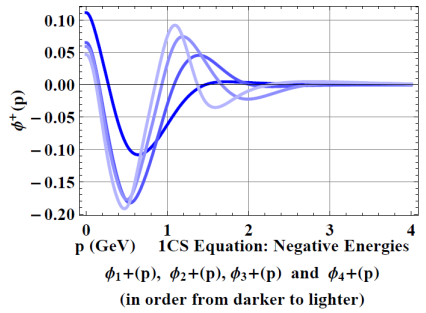

Fig. 16 1CS $\phi^+(p)$ wavefunctions for the first negative energies. The parameters used were: $\sigma = 0.2GeV^2$, $\kappa = 5.0$ and $m_2 = 0.325GeV/c^2$.

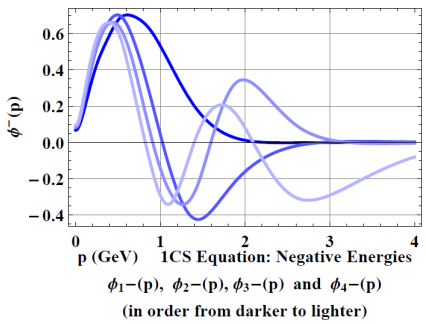

Fig. 17 1CS $\phi^-(p)$ wavefunctions for the first negative energies. The parameters used were: $\sigma = 0.2GeV^2$, $\kappa = 5.0$ and $m_2 = 0.325GeV/c^2$.

n	$\kappa = 1.0$	$\kappa = 5.0$	$\kappa = 10$	$\kappa = 50$	$\kappa = 100$	$\kappa = 1000$	Dirac
4	1.88090	2.11225	2.07724	1.98091	1.96405	1.94787	1.94396
3	1.63183	1.80699	1.78248	1.72044	1.70839	1.69657	1.69493
2	1.29244	1.44224	1.43478	1.40555	1.39956	1.39364	1.39375
1	0.74397	0.93876	0.96313	0.97463	0.97516	0.97543	0.97554
-1	-0.33407	-0.93630	-1.09110	-1.21929	-1.23466	-1.24828	-1.24894
-2	-0.34137	-1.08501	-1.33336	-1.53120	-1.55378	-1.57353	-1.57651
-3	-0.35430	-1.17043	-1.51631	-1.78123	-1.81106	-1.83700	-1.83933
-4	-0.37916	-1.25905	-1.64306	-2.01380	-2.04839	-2.07741	-2.06676

Table 7 Dirac limit of the 1CS equation. The heavy quark mass m_1 is varied in the CST equation. Comparison of the 1CS results for 6 increasing mass ratios with the Dirac results (last column). For these computations m_2 was fixed at $m_2 = 0.325GeV/c^2$. The number of splines used were $SN = 12$.

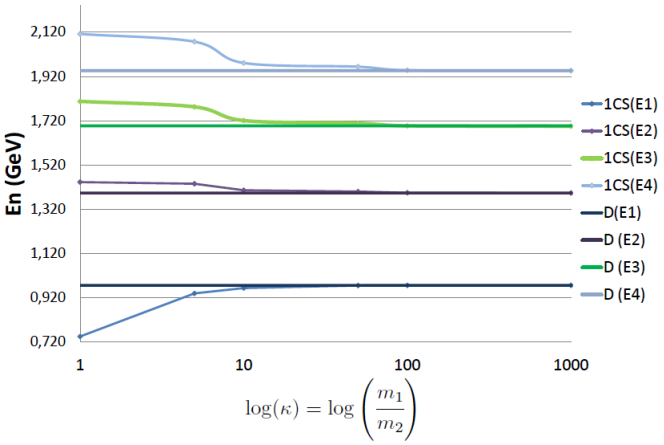

Fig. 18 Dirac limit of the 1CS Equation for the positive energy states. The light quark mass is varied in the CST equation. Comparison of the 1CS with the Dirac results as a function of the quark mass ratio.

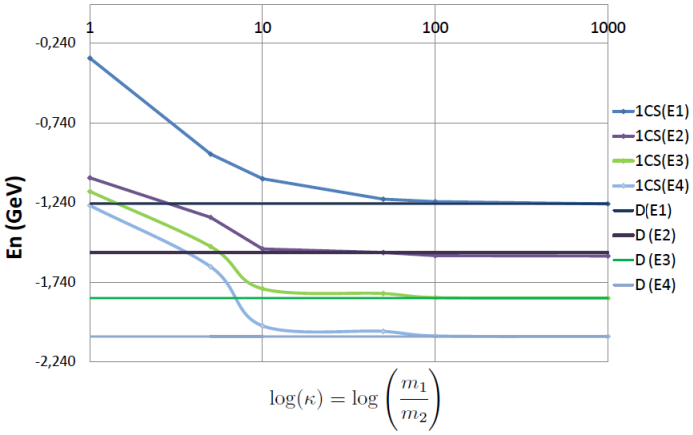

Fig. 19 The same as Fig. 18 but for the negative states.

	SDI	$m_R = 4.65$	$m_R = 10$	$m_R = 20$	$m_R = 100$	$m_R = 1000$
1	2.338108	9.779071	20.37115	40.29458	200.17227	2000.36596
2	4.087949	10.13761	20.64892	40.51505	200.30120	2000.40182
3	5.520560	10.43115	20.87633	40.69555	200.40676	2000.43117
4	6.786708	10.69058	21.07732	40.85507	200.50005	2000.45711

Table 8 Meson masses (in GeV/c^2) according to the NRSE: SDI $SN = 64$.

	$m = 4.65$	$m = 10$	$m = 20$	$m = 100$	$m = 1000$
1	10.27543	20.58412	40.46599	200.28892	2000.14181
2	10.69364	21.02098	40.81371	200.56634	2000.31190
3	10.99657	21.37684	41.12727	200.81554	2000.58749
4	11.24787	21.69625	41.53684	201.03196	2000.96253

Table 9 Meson masses (in GeV/c^2) according to the Dirac equation for increasing m. Parameters: $\sigma = 0.2GeV^2$ and $SN = 12$.

5.2.2.1 Dirac case Another interesting limit to be investigated is when the particle's mass in the Dirac equation increases. We did that and compared it with the NRSE equation results obtained through the SDI Method, for matching parameters. The results are given in tables 8 and 9 and in Fig.20, where the relative difference between the predicted masses in one and the other methods are plotted in terms of $log(m)$. There is one important note in the study of this limit: the values which are being compared are the predicted masses corresponding to the positive solutions of the Dirac equation. The negative eigenvalues still appear in our numerical solutions, but the corresponding eigenvectors tend to zero, as expected. Fig.21 illustrates precisely this.

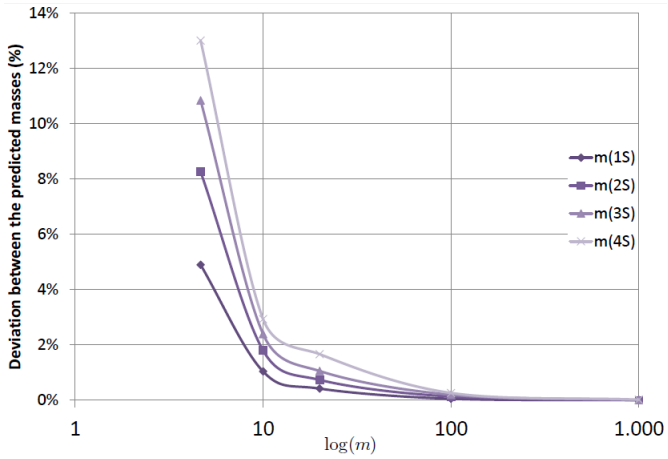

Fig. 20 Non-relativistic reduction of the Dirac Equation. Relative deviations between the Dirac and the Schrödinger equation as a function of the "light" mass for several states.

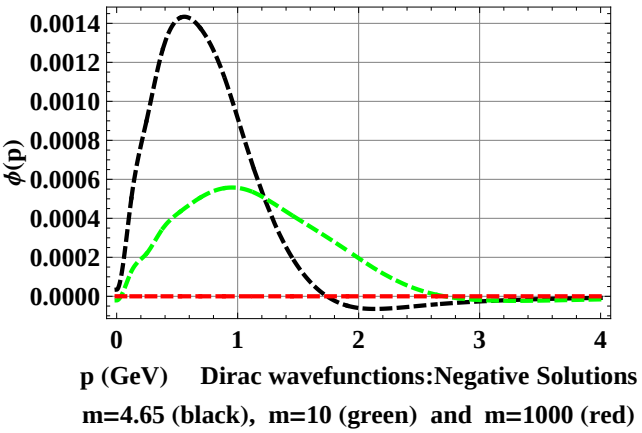

Fig. 21 Dirac wave functions for negative energy states with increasing mass values.

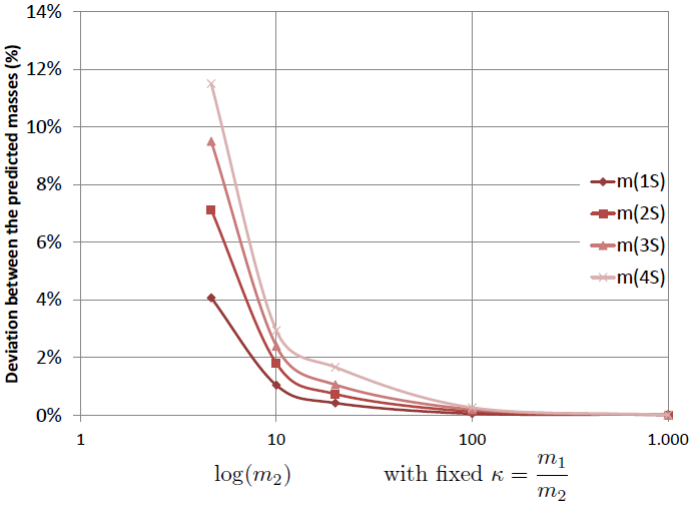

Fig. 22 Non-relativistic reduction of the 1CS Equation. Relative deviations between the 1CS and the Schrödinger equation as a function of the mass for several states

5.2.2.2 1CS case Since we have already shown the one-body (Dirac) limit of the 1CS equation, to show the non-relativistic limit we only have to increase in the latter one the second quark mass. The final results are explicitly shown in table 10 and fig.22.

6 Conclusions and Outlook

This work is the first phase of a phenomenological study of mesons within a relativistic framework, the CST, where the dynamical equation is a quasi-potential equation in momentum space, that is to say, a three-dimensional reduction of the Bethe-Salpeter equation. Quark confinement is obtained by using a linear quark-antiquark potential, whose momentum-

	$m_2 = 4.65$	$m_2 = 10$	$m_2 = 20$	$m_2 = 100$	$m_2 = 1000$
1	9.38050	20.58430	40.46615	200.28900	2000.96253
2	9.41501	21.02132	40.81397	200.56646	2000.58750
3	9.44001	21.37737	41.12751	200.81595	2000.31192
4	9.46075	21.69668	41.53699	201.03214	2000.14185

Table 10 Meson masses (in GeV/c^2) according to the 1CS equation or increasing m_2 and with fixed $\kappa = 1000$. Parameters: $\sigma = 0.2 GeV^2$ and $SN = 12$.

space representation is somewhat subtle, but leads to a rather elegant final equation. Although the fundamental theory QCD is used only to suggest the form of the confining interaction between quarks, the formalism also satisfies another very important feature of hadronic structure: chiral symmetry breaking.

The CST has already been applied to the study of mesons in the past, however, so far the constituent quark mass has been treated as a constant[6,8,9], or as a phenomenological function not related to the kernel[10], and therefore these model calculations are not entirely satisfactory. A consistent implementation of the dynamical breaking of chiral symmetry requires that the dressed quark mass is calculated from the self-interaction of the bare quark through the same confining interaction that acts between the different quarks in a meson. For the special case of the pion, it was shown analytically that, in the chiral limit of vanishing bare quark mass, the two-body CST equation yields a massless pion solution, while the quarks acquire a non-zero dressed mass through dynamical chiral symmetry breaking.

A first step in the implementation of this program was performed in a very recent paper[15], where the quark self-energy in CST was studied for a simple toy model. The next step will be the calculation of the quark self-energy with more realistic interaction models that will then be used to calculate the meson spectrum and the meson wave functions. Moreover, we expect that by connecting the dressed quark mass and the confining interaction we obtain additional useful constraints on the parameters of the interaction model that do not emerge automatically from fits to the spectroscopic data.

A very important part of this program is the development of reliable numerical techniques to solve the CST equations, which have the form of integral equations with a singular kernel in momentum space. The best way to test numerical methods is to apply them to problems where an exact solution is known. For the CST equations no analytic solutions have been found so far, but the numerical solution of integral equations with similar singularities can also be studied with the non-relativistic Schrödinger equation in its momentum-space form. Apart from serving as test problems, the results can also be interesting by themselves, because for heavy-quark systems the non-relativistic description is known to be a good approximation, and a comparison with experimental data becomes meaningful.

In this work, we started with a series of tests of numerical algorithms by solving the non-relativistic differential Schrödinger equation for a linear confining interaction in coordinate space. For s-waves the exact solutions are known analytically, which allows us to estimate the quality of our numerical solutions. The same algorithm is then applied to obtain solutions for higher partial waves, for which no analytic solutions exist, and which can then be used as benchmark values for our numerical solutions of the corresponding integral equation in momentum space.

We proceeded with the solution of the Schrödinger equation in momentum space for the same linear potential. Since its direct Fourier transform does not exist, the linear potential has been used in previous work mostly in a modified, screened form, which introduces a dependence on a screening parameter. An unscreened formulation has been achieved as well in the context of CST calculations. However, in all cases the resulting equations contain a singular kernel. The singularity is of principal-value type and can be integrated, but it requires special treatment and complicates the numerical solution considerably.

The main new contribution of this work is the reformulation of the Schrödinger equation with an unscreened linear potential in momentum space into a form where all singularities are eliminated from the kernel. The numerical solution of this equation requires less effort and computing time than the singular versions. For this purpose we used two different techniques, called SSI and SDI, based on the expansion of the wave function in a basis of B-splines, and compared the results to the corresponding values already obtained in coordinate space. SSI requires single integrations over the kernel multiplied with spline functions, whereas SDI demands the evaluation of double integrals. SSI is much faster than SDI, but for the same number of spline basis functions its results are less accurate then the ones of SDI, which in turn shows a very impressive rate of convergence and overall stability. For some cases with higher partial waves, SSI did not reach a converged result. However, there are ways to improve SSI which we did not yet have time to explore.

We are confident that the method that eliminated the singularities from the nonrelativistic kernel can also be used to do the same in the relativistic kernel of the CST equation. This task is planned for the near future. In this work, we decided to revisit first the work of ref.[14] where the relativistic quark-

antiquark bound-state problem was solved in a somewhat simplified form (retardation was neglected) with the Dirac and 1CS equations. We obtained very good agreement of our results for the bound-state energies, which in the relativistic case are both positive and negative, with the results reported in ref. [14].

In addition to these tests that confirm the validity of our numerical methods, we checked whether the solutions of the 1CS and Dirac equations behave as expected in certain limits. First, in the limit of one mass tending to infinity, the 1CS results should become equal to the Dirac results. This is called the one-body limit, and by fixing one quark mass and making the other one heavier and heavier, i.e. by increasing the mass ratio, we see that the bound-state energies indeed converge towards the Dirac energies. In fact, the 1CS equation works particularly well for the description of heavy-light quark systems, where it is expected to be a very good approximation for the more general two-channel CST equation.

Second, in the limit of all quark masses becoming very large, both relativistic equations should approach the same nonrelativistic limit, namely the Schrödinger equation. Again, we find that the numerically obtained energies of the Dirac and 1CS equations indeed tend towards the Schrödinger energies when the quark masses are increased. It also confirms that our relativistic generalization of the linear potential behaves correctly in the nonrelativistic limit.

We believe that this work will enable us to increase the efficiency of computer codes required to solve more realistic models involving a linear confining interaction within the CST framework in the near future. We are particularly interested in the light quark systems, where relativistic effects are large, and where a two-channel CST equation (2CS) has to be applied. Once a parametrization of the interaction model is found that provides a good description of the meson spectrum, the corresponding meson wave functions can be used to calculate many interesting properties of the mesons themselves or of reactions in which they participate.

References

1 F. Jegerlehner, A. Nyffeler, Phys. Rept. **477**, 1 (2009)
2 B. Friman, C. Höhne, J. Knoll, S. Leupold, J. Randrup, R. Rapp, *The CBM Physics Book: Compressed Baryonic Matter in Laboratory Experiments. Lecture Notes in Physics* (Springer, 2011)
3 F. Gross, Phys. Rev. D **186**, 1448 (1969)
4 F. Gross, Phys. Rev. C **26**, 2203 (1982)
5 F. Gross, Phys. Rev. C **26**, 2206 (1982)
6 F. Gross, J. Milana, Phys. Rev. D **43**, 2401 (1991)
7 A. Stadler, F. Gross, Few-Body Syst. **49**, 91 (2011)
8 F. Gross, J. Milana, Phys. Rev. D **45**, 969 (1992)
9 F. Gross, J. Milana, Phys. Rev. D **50**, 3332 (1994)
10 C. Savkli, F. Gross, Phys. Rev. C **63**, 035208 (2001)
11 S. Godfrey, N. Isgur, Phys. Rev. D **32**, 189 (1985)
12 Y. Nambu, G. Jona-Lasinio. Phys. Rev. **122**, 345 (1961); Phys. Rev. **124**, 246 (1961)
13 F. Gross, *Relativistic Quantum Mechanics and Field Theory* (Wiley - InterScience, 1999)
14 M. Uzzo, F. Gross, Phys. Rev. C **59**, 1009 (1999)
15 E. Biernat, F. Gross, T. Pena, A. Stadler, Few-Body Systems (2012)